Limits of metastable epitaxy: The structure of ultrathin Fe films on $Cu_3Au(100)$

B. Schirmer
Institut für Grenzflächenforschung und Vakuumphysik, Forschungszentrum Jülich, D-52425 Jülich, Federal Republic of Germany

B. Feldmann
Institut für Grenzflächenforschung und Vakuumphysik, Forschungszentrum Jülich, D-52425 Jülich, Federal Republic of Germany and Booz Allen & Hamilton, D-40215 Düsseldorf, Federal Republic of Germany

M. Wuttig
Institut für Grenzflächenforschung und Vakuumphysik, Forschungszentrum Jülich, D-52425 Jülich, Federal Republic of Germany and I. Physikalisches Institut, Rheinisch-Westfälische Technische Hochschule Aachen, D-52056 Aachen, Federal Republic of Germany

(Received 6 January 1998; revised manuscript received 12 March 1998)

The influence of epitaxial strain on the structure of thin films was investigated using a model system: Fe on $Cu_3Au(100)$. Low-energy electron diffraction (LEED) $I(V)$ measurements and full dynamical $I(V)$ calculations were used to determine the atomic structures of Fe films at different thicknesses (3.3, 4.8, 18, and 53 monolayers (ML). LEED measurements show that for thicknesses above approximately 1.5 ML iron films are no longer pseudomorphic. Between 3.3 and 4.8 ML, the Fe films were determined to have a strained bcc structure, rather than the previously proposed fcc structure. The existence of the strained bcc phase at low coverage is consistent with estimates of the total energy, which suggests that the energy gained by stabilizing the bulk ground state of Fe overcompensates the higher strain energy of the bcc phase. At higher film thicknesses, 18–53 ML, dynamical LEED $I(V)$ analysis confirm that the film structure has evolved into the expected unstrained bcc structure of Fe. [S0163-1829(98)01932-8]

I. INTRODUCTION

The discovery of a giant magnetoresistance (GMR)[1,2] in ultrathin ferromagnetic films coupled through a nonmagnetic spacer layer has spurred interest in magnetic thin films and interfaces. To fully exploit this effect, it would be useful if for a given substrate/film combination, the structural and magnetic properties of the film could be predicted with high reliability. To understand the challenges of such an endeavor, one needs to consider the various contributions that influence film structure. Calculating the ground-state structure of certain magnetic elements such as iron or manganese is already a considerable task for bulk samples at $T=0$K, since the energy differences between different structural and magnetic phases are often below 0.1 eV/atom. For thin films a number of additional contributions need to be considered that can stabilize a phase that would be unfavorable in the corresponding bulk sample. The energetic contribution of the film surface and the film/substrate interface is often of the order of 0.2 eV/atom. Unfortunately these quantities are difficult to determine experimentally. Furthermore, the misfit between the deposited film and the substrate plays a major role and can easily add energies of 0.1 eV/atom. This quantity can at least be estimated with some precision using the known elastic properties of bulk samples.[3] Furthermore thin film stresses can also be determined experimentally with considerable precision.[4] Hence the influence of film stress on the resulting energy of the ground state can be studied. Jona and Marcus were the first to discuss the concepts required to predict the influence of film strain on the stability of metastable states.[5]

The most interesting candidates to explore the effects of film stress on film structure are those materials that already show a rich variety of bulk phases depending upon pressure and temperature. Iron is a prime example since it shows a rich variety of structural and magnetic phases and thus offers ideal testing grounds to confirm the ability of influencing film structure by using different substrates.[6–12] Indeed, it was possible to create different structural and magnetic states of Fe depending on the lattice parameter of the substrate. For Cu(100) and related systems like Ni/Cu(100) (Refs. 13 and 14) and Co/Cu(100) (Refs. 15 and 16) an fcc high spin state with an atomic volume of $V_a=12.1\text{Å}^3$ was stabilized for Fe-film thicknesses up to 5 ML.[8] For coverage between 5 and 11 ML all iron layers except the top layer are unreconstructed and have a smaller atomic volume of $V_a=11.4\text{Å}^3$.[8–10] These layers presumably show antiferromagnetic coupling.[8,10] The top layer is reconstructed in $p2mg(2\times1)$ symmetry and shows a high spin FM state with an enlarged volume of 12.1 Å^3.[6,9,10] Above 11 ML, iron grows in a bcc modification where the (110) surface plane is parallel to the (100) substrate surface.[17,18] On the other hand, Fe films on Ag(100) (Refs. 19 and 20) or Au(100) (Ref. 21) have a nearly perfect bcc structure even for the initial growth stage. This phenomenon is understandable considering the misfit for the different structures. The lattice parameter for FM fcc Fe can be extrapolated to 3.65 Å from high-spin, ferromagnetic fcc Fe alloys. This corresponds to 2.58 Å for the edge of the primitive square. bcc Fe has a lattice constant of 2.87 Å. The lattice parameter of Cu(100) is 3.61 Å, while Ag and Au have lattice spacings of 4.07 and 4.08 Å (edge of the primitive square 2.88 Å both), respectively. The misfit is defined as $f=(a-a_0)/a_0$, with a_0 and a being the in-plane nearest-neighbor distance of the film and the substrate, respectively. The misfit between Cu(100) and the fcc modification of Fe is just 1.1%, which is far less than the misfit for the bcc Fe modification. This can compensate for the fact that the energy of the fcc state is higher. Only for larger film

thicknesses, a structural transition to bcc iron is observed. For Ag and Au substrates, on the contrary, the misfit for the bcc iron modification is with 0.2 and 0.5% rather small, enabling the growth of this phase. Hence, we expect a phase transition from fcc to bcc iron for substrate lattice spacings between 3.61 and 4.07 Å. The precise determination of the substrate lattice spacing where a phase transition from fcc to bcc iron is observed would allow a better estimate of the contribution of stresses to the total energy. Rh has a lattice constant of 3.80 Å, which is almost half-way between the lattice constants of Cu and Ag. Conflicting results have been obtained for the structure of Fe films on Rh(100). While a full-dynamical low-energy electron diffraction (LEED) $I(V)$ study determined the film structure to be bcc,[22] an angle-resolved Auger electron spectroscopy and LEED study concluded that in the initial growth stage fcc iron is stabilized.[23] However, it is generally accepted that full-dynamical LEED analyses should give much more reliable structural data. Hence, iron films on Rh(100) presumably have a bcc structure.

Unfortunately there are no metallic elements with an fcc structure and a lattice spacing between 3.61 and 3.80 Å. An interesting alternative has already been explored previously by Gradmann.[7] He determined the magnetic properties of deposited iron films on Cu_xAu_{1-x} alloys with varying composition and hence lattice spacing. These properties showed profound changes with alloy composition. However, these changes could not be related unequivocally to different structural states.[7,24]

We have chosen Cu_3Au (100) as a model substrate in this study in part because this alloy has a lattice constant of 3.75 Å. Interestingly enough, a number of studies have already investigated iron films on this substrate.[5,25–27] Most studies have focused on the magnetic properties of the films. Ferromagnetism was observed for film thicknesses above 1.1 ML.[25,26] A spin reorientation transition from perpendicular to in-plane at a thickness of 5.5 ML has recently been reported.[26] Previous studies had already speculated about such a magnetic reorientation.[25] This transition has been attributed to a structural transformation from fcc to bcc iron.[26] While similar conclusions have been derived from several studies, those investigations only analyzed the LEED pattern and performed a kinematic analysis of LEED $I(V)$ data.[25,26] Recently, Lin *et al.* have also used STM to support these findings,[26] while a previous full-dynamical LEED analysis turned out to be inconclusive.[27] This leaves us with the interesting situation that while on Rh(100) with a lattice spacing of 3.80 Å bcc iron is stabilized, on $Cu_3Au(100)$ with a lattice constant of 3.75 Å apparently the fcc iron modification can be grown up to 5.5 ML before a transformation to bcc iron occurs. This switching thickness is even larger than for Cu(100), where the ferromagnetic fcc state can only be stabilized up to 5 ML.[8] Switching thickness on Cu_3Au depends upon the growth temperature of the films and has been determined to 3.5 ML for growth at 300 K and 5.5 ML for 160-K growth. We observe a reorientation transition at 2.3 and 3.2 ML for growth at 300 and 150 K (Ref. 28), respectively.

To test these conclusions and to precisely determine the crystallographic structure of the iron films, we have performed an extensive study of the film structure for Fe on $Cu_3Au(100)$. Our findings will be compared with predictions based on recent calculations for the energy of different iron states employing concepts which were put forward by Jona and Marcus.[3,5] The paper is organized as follows. In the second section we give a brief description of the experimental setup and theoretical procedures. Our results are presented in the third section. In the fourth section a discussion and comparison with previous results can be found. The paper ends with a conclusion and summary.

II. EXPERIMENT

The experiments were performed in an ultrahigh vacuum chamber containing several possibilities for preparation and analysis of thin films. These tools allow the determination of growth, structure, and magnetism of surfaces and thin films. Both the apparatus and our treatment of the Cu_3Au single crystal have already been described elsewhere.[29] The $Cu_3Au(100)$ single crystal was cleaned by several sputtering and heating cycles. The preparation included extensive annealing cycles as described in Ref. 28 to obtain the sharpest possible LEED pattern. In addition, Auger spectroscopy was used to control the contamination level. Sputtering and heating cycles were continued until no contamination could be observed any more. After this procedure high-purity Fe (99.99%) was evaporated from a small disk by radiation. During Fe deposition the pressure rise was typically below 1×10^{-8}Pa. After the deposition source was turned off, it quickly dropped to the base pressure of 4×10^{-9}Pa. The growth was studied by monitoring the MEED intensity during deposition and later by determining the Auger intensity ratios. As described elsewhere[28] the thickness determination by MEED has a precision of 8% and was in excellent agreement with the thickness determination by Auger intensity ratios. This allows a precise determination of film thickness and enables a detailed correlation of film structure and magnetic properties with thickness.

For the precise determination of film structure the energy dependence of the intensities of several LEED beams was measured and compared with full dynamical calculations for several film thicknesses. LEED spot profiles were measured in addition to analyze the surface morphology and superstructure evolving with increasing film thicknesses.

In this study a sample manipulator was employed that allows a precise variation of the polar and the azimuthal angle but not the tilt, which was fixed. The corresponding angle has to be determined separately in the course of the LEED optimization.[9] A program developed by Moritz was used[30] for the calculation of LEED intensities. In this program symmetry adapted functions are used to reduce the angular momentum components and the layer doubling method is employed to stack the layers. The best fit is determined by a standard grid search. The atomic scattering is described with a maximum of 10 phase shifts derived from band-structure calculations.[31] In the calculations it was assumed that the iron films have an infinite thickness, i.e., the scattering from the $Cu_3Au(100)$ substrate was neglected. This is a reasonable assumption for thicker films, but will reduce the accuracy of the structure determination for films with thicknesses below 5 ML. Both the imaginary part of the inner potential, which describes the electron attenuation, and the

real part of the inner potential are determined by the theory-experiment fit minimizing two different R factors, namely, the Pendry R factor[32] (R_p) and the R_{DE} R factor.[33]

III. RESULTS

A. Growth

We have observed that the magnetic properties of the deposited iron films depend not only upon thickness but also on the substrate temperature during deposition.[28] The differences could be attributed mainly to interface roughness, which depended on the growth temperature of the films. In addition, segregation of substrate atoms[28] was found. For a preparation temperature of 150 K, no segregation of Cu and Au to the film surface is observed after iron deposition. For a growth temperature of 300 K (RT), on the contrary, a predominant diffusion of Au atoms is observed. For iron film thicknesses up to 4.4 ML, Auger spectroscopy observes Au in the surface vicinity. The thin iron films in this study were typically deposited at room temperature (300 K) but the thinnest were deposited partially at low temperature (150 K) to avoid segregation.

B. Structure

The structure of the Fe films on Cu_3Au was characterized by LEED, including the measurement of LEED $I(V)$ curves. Superstructure spots were observed by LEED for 150 K (LT) and 300 K (RT) preparation. The superstructure spots occur in a thickness range from 1.2 to 3 ML for LT deposition and 1.8 to 5.5 ML for RT deposition. The superstructure spots are less intense for LT growth than for RT growth. The difference in the thickness is caused by the growing surface roughness in LT films above 3 ML. A spot profile analysis at 1.8 ML revealed for LT and RT growth that the superstructure is either a $(n\sqrt{2}\times 1)R45$ or a $(n\sqrt{2}\times n\sqrt{2})R45$ structure with $n=13$–14. The superstructure spots converge towards the integer order spots for larger thicknesses. A spot profile analysis for a 4.8 ML RT film shows the same superstructure with $n=33$. The effect of increasing n can be explained by a growing superstructure unit cell. Only superstructure spots near integral order beams ($k\pm 1/n$, $l\pm 1/n$) including ($k=l=0$) are observed. This limits the number of models to a sinusoidal displacement of atoms in the direction of the surface normal, i.e., a corrugation of n atoms in the fcc [001] direction. Because the superstructure spots do not exhibit a preferential streaking in any crystallographic orientation we cannot distinguish if the atoms are corrugated in a wave form in the fcc [010] direction or in both the fcc [010] and fcc [100] direction.

The intensity of two neighboring superstructure spots is unsymmetrical with respect to the adjacent substrate spot. The most intense superstructure spots are always observed for the negative sign, i.e., $(k-1/n,l-1/n)$. This behavior is expected if the characteristic interatomic spacing in the scattering plane is larger than the Cu_3Au in-plane nearest-neighbor spacing. We conclude that the characteristic in-plane atomic spacing in the Fe layer is 3–6% larger than the atomic spacing in the Cu_3Au surface of 2.65 Å (Ref. 28) in the thickness range up to 5.5 ML. Above 6 ML, the intensity of the substrate beams decreases. They are no longer visible above 9 ML.

The LEED data presented above describe the appearance and evolution of superstructures with growing thickness. This gives a first hint of the film structure and structural changes with film thickness but is insufficient to determine the full structure, i.e., the precise atomic positions in the Fe layers. To achieve this goal, LEED $I(V)$ curves have been recorded for a number of Fe films. Both film thicknesses and preparation conditions were varied to determine the influence of the film thickness and preparation on film structure. The selection of Fe layer thicknesses represents a cross section over the relevant thickness range. In the following we will present results with decreasing film thickness starting with a 53-ML-thick film. We continue with a 18.7 ML film. Finally we have investigated a 4.8-ML- and a 3.3-ML-thick film to cover the thin film limit, as well. The 53-ML film was deposited at 300 K and afterwards annealed up to 470 K. The 18.7-ML-thick film was also deposited at 300 K but not annealed afterwards. To deposit the 4.8-ML film, at first 2 ML were deposited at 150 K to avoid interdiffusion and afterwards 2.8 ML were evaporated at 300 K. Subsequently the film was annealed up to 470 K. The thinnest Fe film was obtained by deposition of 1.2 ML at 150 K following 2.1 ML at RT without annealing.

Various parameters were varied independently to successfully fit the experimental data. The optimized parameters can be divided in two groups. The first group contains the structural parameters. Interlayer spacings were varied for the first three layers. Furthermore both the bulk interlayer spacing (d_b) and the in-plane nearest-neighbor spacing (a_p) were optimized to account for strain relaxation. The precise determination of these parameters is most crucial for the structure determination of thin films. Furthermore nonstructural parameters were optimized including, as mentioned above, the imaginary (V_i) and the real part (V_0) of the potential. Also included were the Debye temperatures, which were varied independently for the surface and the bulk of the iron film. Finally the tilt was determined to be $1.35°\pm 0.2°$. The tilt is identical for all films investigated because all layers have been deposited on the same single crystal. For the precise determination of film structures error bars need to be determined as well. Our estimate for the error bar comes from the variance of R, $\mathrm{var}(R_p)=R_p*\sqrt{8V_i/\Delta E}$, where ΔE is the range of energies where calculated and measured spectra overlap. The energy overlap is 2680 eV for the 53-ML-thick film, 1975 eV for the 18-ML-thick film, 2824 eV for the 4.8-ML-thick film and 2832 eV for the 3.3-ML-thick film.

Figure 1 shows measured $I(V)$ curves for the 53-ML film and calculated $I(V)$ curves for the best fit for five representative beams. The comparison between experimental and calculated curves shows a good agreement for both the peak positions and the peak forms, indicative for a low R factor. Table I lists the best-fit structure for the 53-ML Fe film, which is $d_{12}=1.48\pm 0.03$ Å, $d_{23}=1.47\pm 0.02$ Å, $d_b=1.455\pm 0.02$ Å, and $a_p=2.86\pm 0.05$ Å. This shows that the film has a nearly perfect bcc Fe structure ($d_b=1.435$ Å and $a_p=2.87$ Å). The best-fit parameters obtained for the different R factors R_p and R_{DE} agree to better than 0.01 Å. Our conclusion is in accordance with previous studies, employing a kinematical analysis of LEED data,[25,26] which concluded that at large film thicknesses bcc iron is stabilized.

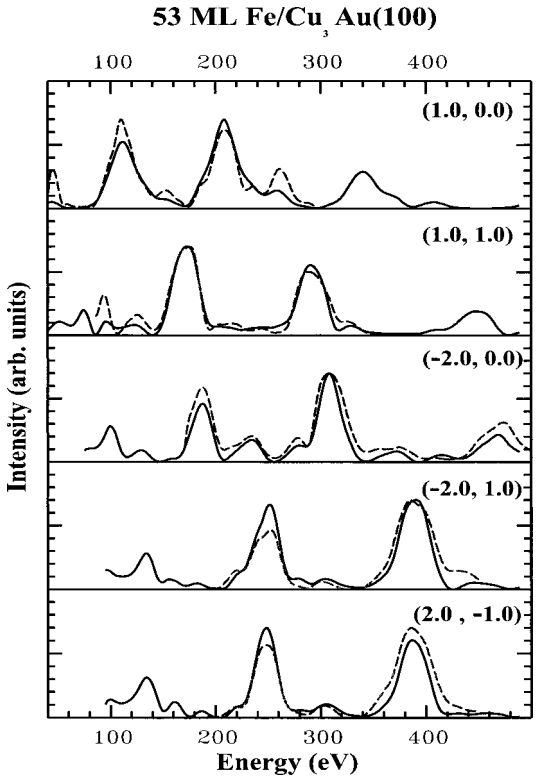

FIG. 1. Comparison of calculated $I(V)$ curves for the best fit model (solid lines) and experimental $I(V)$ curves (dashed lines) for the 53-ML-thick Fe film. The film was deposited at 300 K and annealed up to 470 K after the deposition. Experimental and calculated curves show a very good agreement in both peak position and peak form.

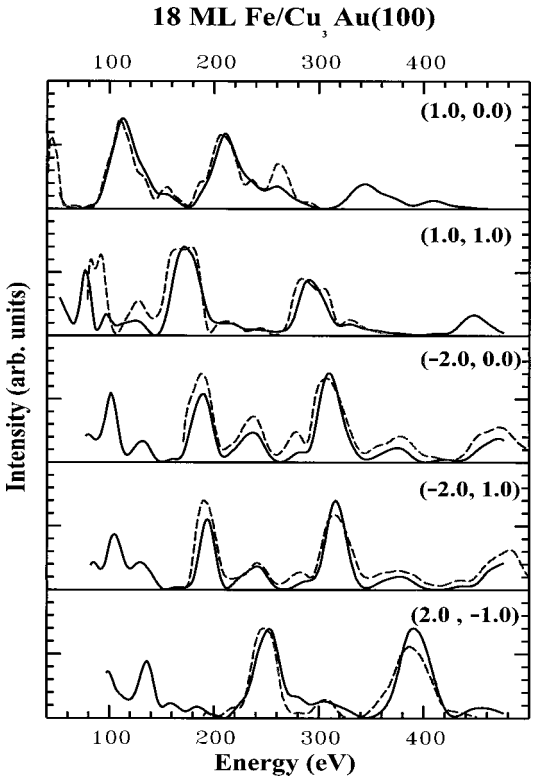

FIG. 2. Comparison of experimental (dotted lines) and calculated (solid lines) $I(V)$ curves for the 18-ML-thick film deposited at 300 K. With the exception of the (1,1) beam, all curves show a very good agreement.

Figure 2 shows an experiment/theory comparison for the 18.7-ML-thick Fe film. This film was not annealed after preparation. Therefore the roughness of the film was higher, which reduced the intensity and increased the width of the LEED spots. Therefore fewer LEED spots were recorded than for the other film thicknesses. This smaller database tends to increase the error bar as mentioned above. Nevertheless Fig. 2 shows that the agreement between calculated and experimental data is as good as for the 53-ML film. Even the R factors are similar. The structural parameters are $d_{12}=1.45\pm0.02$ Å, $d_{23}=1.48\pm0.03$ Å, $d_b=1.46\pm0.03$ Å, and $a_p=2.83\pm0.055$ Å. Again, we hence observe a bcc-like structure but this time with a slightly larger tetragonal distortion.

TABLE I. Optimum parameters for R_p for the different Fe film thicknesses. d_{ij} is the interlayer distance between layer i and j, Θ_{Di} is the Debye temperature of layer i, and a_p is the in-plane nearest-neighbor spacing. The index b denotes the bulk parameter while ΔE is the energy overlap between calculated and experimental $I(V)$ curves.

Parameter	3.3 ML	4.8 ML	18 ML	53 ML
R_p	0.307	0.294	0.270	0.271
d_{12}(Å)	1.57±0.03	1.56±0.02	1.45±0.02	1.48±0.03
d_{23}(Å)	1.51±0.03	1.505±0.02	1.48±0.03	1.47±0.02
d_b(Å)	1.53±0.05	1.51±0.025	1.46±0.03	1.455±0.02
a_p(Å)	2.72±0.06	2.74±0.055	2.83±0.055	2.86±0.05
Θ_{D1}(K)	480	300	460	400
Θ_{D2}(K)	520	470	470	400
Θ_{Db}(K)	520	500	550	400
ΔE(eV)	2832	2824	1975	2680

The experiment/theory comparison for the 4.8-ML film is shown in Fig. 3. The film was annealed after preparation to decrease the film roughness and improve the order. Figure 3 again shows a good correspondence between theoretical and experimental data. This results in small error bars of ±0.025 Å for structural parameters such as d_b. The structural parameters for this thickness are $d_{12}=1.56\pm0.02$ Å, $d_{23}=1.505\pm0.02$ Å, $d_b=1.51\pm0.025$ Å, and $a_p=2.74\pm0.055$ Å. Obviously the Fe film has a much larger tetragonal distortion. This shows that the influence of the substrate is much higher for the 4.8-ML Fe than for higher coverage. Interesting enough, the LEED $I(V)$ analysis reveals that the in-plane lattice spacing is larger than the in-plane lattice spacing of Cu_3Au. This agrees nicely with the 3% lattice expansion we derive from the analysis of LEED superstructure spots for a similar thickness.

Figure 4 shows the measured and the calculated $I(V)$ curves for the 3.3-ML thin film. The precise reproduction of the measured LEED $I(V)$ curves through the computation of LEED data is a considerable challenge for several reasons. Due to the film roughness, the LEED spots are somewhat weak and diffuse, leading to low intensities in the experimental data. Then, for such a thin film it is difficult to ignore the influence of the substrate. Nevertheless, a full dynamical analysis assuming infinite film thickness is still superior to a

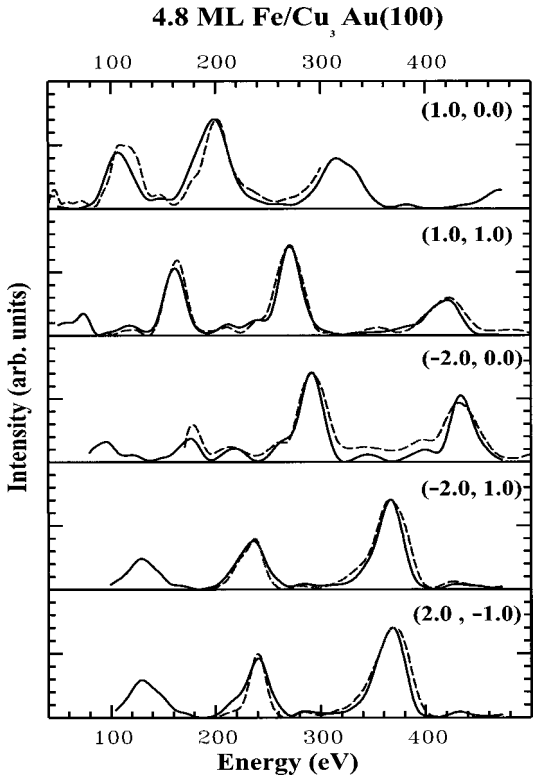

FIG. 3. The dotted curves denote the experimental $I(V)$ curves and the solid curves the best-fit structure calculated for the 4.8-ML-thick film. To suppress the influence of the Au diffusion the first 1.6 ML were deposited at 150 K and the last 3.2 ML at 300 K. The film was annealed up to 470 K after the deposition.

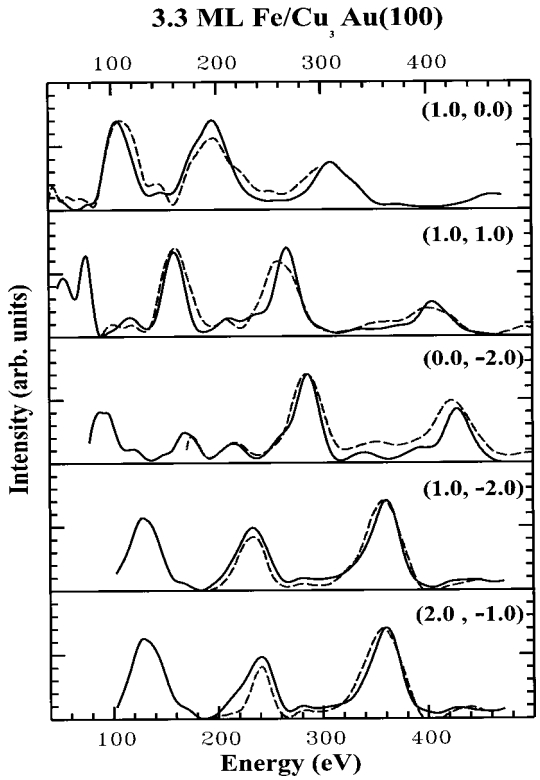

FIG. 4. Same as before, but for the 3.3-ML-thick Fe film. This film was also deposited in two steps. The first 1.2 ML were deposited at 150 K and the last 2.1 ML Fe at 300 K.

kinematical LEED analysis. The surprise is that despite these difficulties the agreement between theory and experiment is only slightly worse than for the other film thicknesses. Nevertheless, this results here in a noticeably larger error bar for the structural parameters than for the other coverage. The optimized structural parameters are $d_{12}=1.57\pm0.03$ Å, $d_{23}=1.51\pm0.03$ Å, $d_b=1.53\pm0.05$ Å, and $a_p=2.72\pm0.06$ Å. The Fe film with a thickness of 3.3 ML hence displays an even larger tetragonal distortion then the 4.8-ML-thick film. Note that $a_p=2.72$ Å is again larger than than the in-plane lattice constant of Cu_3Au($a_p=2.65$ Å), similar to our finding for the 4.8-ML-thick film and the analysis of LEED spot profiles.

Figure 5 shows the variation of R_p with the bulk interlayer spacing d_b and the in-plane nearest-neighbor distance a_p. From the dependence of the position of the R-factor minimum upon thickness one can follow structural changes with increasing film thickness. These plots have additionally been used to determine the error bar for d_b and a_p.

From the information described above we will derive in the next section the ground-state structure as a function of increasing film thickness and correlate the film structure to previously reported magnetic properties.

IV. DISCUSSION

In the last few years, several groups have studied the structure and magnetism of Fe on $Cu_3Au(100)$. These studies consistently observe ferromagnetism in Fe films thicker than approximately 1.1 ML. Close agreement also exists for the film structure at large thicknesses of more than 10 ML. Previous studies already derived the bcc structure of these films from a kinematic analysis of the $I(V)$ curve for the (0,0) beam. This structure is confirmed by our full dynamical analysis of several beams, which determine that the in-plane lattice constant a_p is 2.86 Å and the bulk interlayer spacing is 1.455 Å for a 53-ML-thick film. These values closely resemble the atomic distances of bcc iron. The bulk interlayer spacing of bcc iron with (100) surface orientation is 1.435 Å, a_p is 2.87 Å. A similar structure is found in our full dynamical analysis for an 18-ML-thick film with a_p of 2.83 Å, and d_b of 1.46 Å. Therefore, these findings unequivocally confirm the bcc structure at large film thicknesses.

In the case of thinner Fe films, however, the situation is more complex. Previous studies performed a kinematic analysis of the (0,0) beam and determined an interlayer spacing of 1.89–1.98 Å. From this interlayer spacing it was concluded that fcc iron is stable at small thicknesses up to 5.5 ML. We have measured the $I(V)$ curve of the (0,0) beam for 3.3- and 4.8-ML-thick iron films. The data for the (0,0) beam were used as input for a full dynamical LEED analysis. This analysis showed two minima, one for the film structure as determined by Lin *et al.*, i.e., $d_b=1.875$ Å. A second R-factor minimum is found for $d_b=1.53$ Å and $a_p=2.74$ Å, i.e., data very similar to the best-fit structure of an extensive data set shown in Fig. 3. Hence the determination of the film structure based on the data for the (0,0) beam alone is inconclusive (see Fig. 6). Therefore we tried to fit our entire data set of 10 beams for the 3.3-ML-thick iron film with the structural parameters derived by Lin *et al.*[26] The

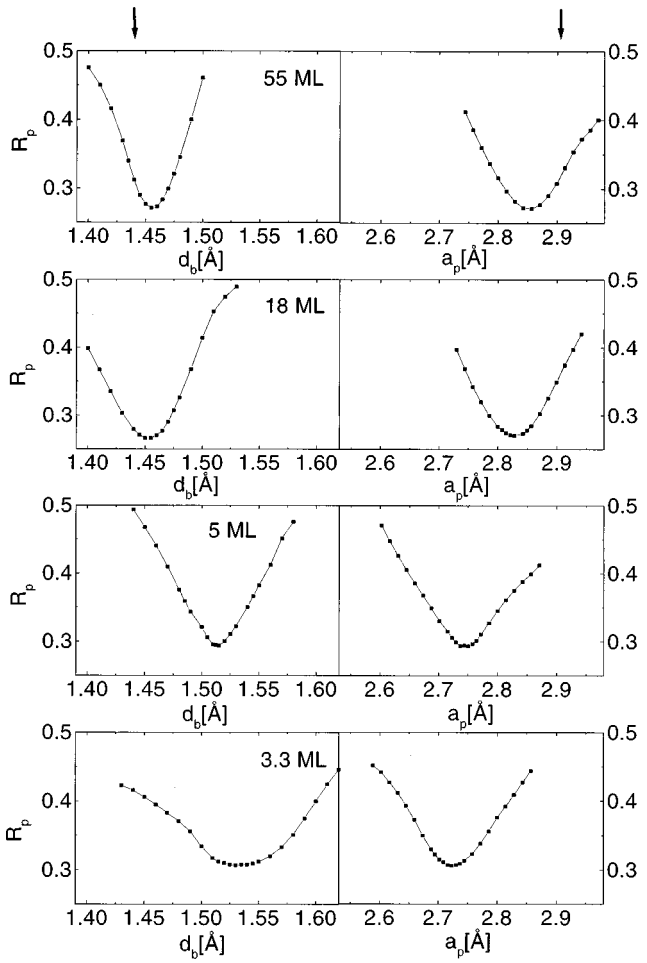

FIG. 5. The figure shows the dependence of the Pendry R factor upon the variation of the bulk interlayer distance and the in-plane nearest-neighbor spacing. The sharp and deep minima allow a precise determination of the film structure. Because of the broader minimum for the 3.3-ML film the error bar is larger for this film thickness. The arrows denote the bulk interlayer distance d_b and the in-plane nearest-neighbor spacing a_p for bulk bcc(100) Fe.

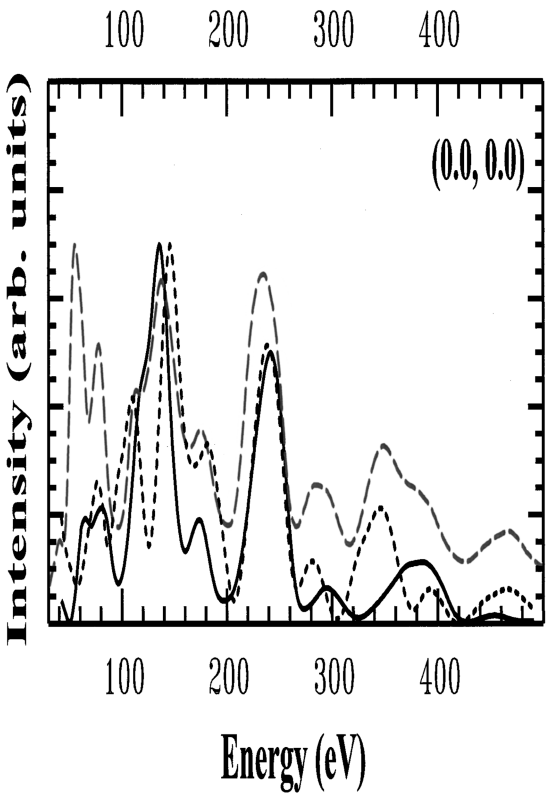

FIG. 6. In this figure the fcc and the bcc model are compared with the experimental data for the (0,0) beam for 3.3 ML. The long-dashed line shows the experimental data, the solid line the bcc model, and the short-dashed line the fcc model. For both models a tilt of 7 ° was assumed.

resulting $I(V)$ curves are shown in Fig. 7. A visual inspection reveals that neither the peak forms nor the peak positions are satisfactorily reproduced by the calculated $I(V)$ curves. This is confirmed by the unsatisfactorily high R factor of 0.666. We have to conclude therefore that the structural parameters of Lin *et al.* are only sufficient to reproduce the $I(V)$ curve of the (0,0) beam but not the full data set and hence do not describe the true film structure.

Figure 8 shows the values for d_b and a_p for the four different iron film thicknesses we have studied on $Cu_3Au(100)$. For comparison the bulk interlayer spacing d_b and nearest-neighbor spacing a_p of FM (large circle) and AFM fcc (large rhombus) iron and bcc iron (large square) are shown as well. Even though the structural parameters we determine are closest to the bcc structures, this is not conclusive evidence that the films have indeed bcc structure. We have to instead determine the structure of the film assuming the film would not be strained by the substrate. This unstrained, equilibrium film structure can be obtained from the epitaxial line[3,5] under two assumptions. The elastic properties of the thin films have to be independent of film strain, which is reasonable at least for small misfits and they can be described by bulk elastic constants. Then the equation between c and a, where c is twice the interlayer spacing (d_b), and a is the nearest-neighbor spacing in the plane, can be derived to $c/c_0=(a/a_0)^{-\gamma}$, where $\gamma=2\nu/(1-\nu)$, ν being the Poisson ratio. In Fig. 8 the epitaxial line for the three states of iron are displayed. The structural parameters we have determined are closest to the epitaxial line of bcc iron. The antiferromagnetic fcc solution has to be excluded, since these as well as previous measurements show that the iron films are ferromagnetic. This finally proves that iron films on $Cu_3Au(100)$ have a bcc structure at least above 3.3 ML and presumably even below this thickness. Additional confirmation for this conclusion comes from the observed LEED pattern, which reveals that the iron atoms have a nearest-neighbor spacing that is enlarged by 3–6 % compared to the $Cu_3Au(100)$ substrate. This interatomic spacing is sketched by the shaded ellipse in Fig. 8. Such an increased nearest-neighbor spacing would be highly implausible for the growth of the fcc modification, which has an equilibrium spacing of 2.57 Å. The film structure determined by Lin *et al.* is also displayed in Fig. 8. The corresponding data point is far away from any epitaxial line.[26] This problem has already been realized by Lin *et al.* and was attributed to an extremely large atomic volume. We have shown above that the corresponding film structure cannot account for the observed LEED $I(V)$ curves and has to be excluded. Furthermore, we believe that the bcc interlayer spacing and the observed strain relief

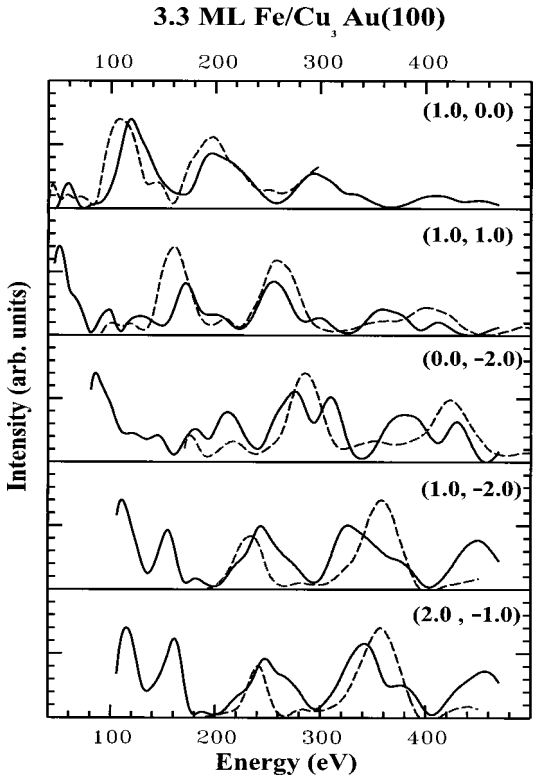

FIG. 7. Comparison of experimental (dotted lines) and calculated (solid lines) $I(V)$ curves for the 3.3-ML-thick film using the parameters ($d_{12}=2.03$ Å, $d_{23}=1.99$ Å, $d_b=1.875$ Å, and $a_p=2.65$ Å) taken from Ref. 26. The nonstructural parameters were the same as used in Fig. 4. Both the calculated peak positions and the peak forms do not agree very well with the experimental data. This indicates that the structural parameters listed above do not describe the film structure properly.

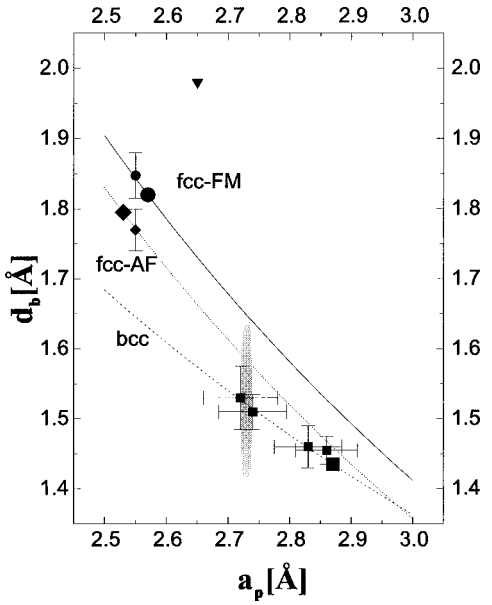

FIG. 8. The different structures for various bulk phases of iron are depicted FM bcc Fe ($d_b=1.435$ Å, $a_p=2.87$ Å) (large full square), FM fcc Fe ($d_b=1.82$ Å, $a_p=2.57$ Å) (large full circle) and AF fcc Fe ($d_b=1.795$ Å, $a_p=2.53$ Å) (large full rhombus). In addition, the three curves show the epitaxial lines for FM bcc Fe (dashed line), FM fcc Fe (solid line) and AF fcc Fe (dotted line). The epitaxial lines were calculated using the formula $d/d_{\mathrm{eq}}=a/a_{\mathrm{eq}}{}^{-\gamma}$ (see also [3]). For the calculation, a parameter $\gamma_{\mathrm{bcc}}=1.16$ and $\gamma_{\mathrm{fcc}}=1.64$ was used. Our structure determination for 3.3-ML, 4.8-ML, 18-ML, and 53-ML thick films is displayed as well including the error bars (small full rhombus). It is clearly visible that the epitaxial line for the bcc structure gives an excellent fit to the film structure for the entire thickness range studied. This is not the case for the FM fcc line. The AF fcc line can be excluded since the films investigated here show ferromagnetism over a wide thickness range. The shaded area between a_p of 2.72 and 2.74 Å depicts the in-plane nearest-neighbor spacing derived from an analysis of LEED spot positions. This analysis does not allow for the simultaneous determination of interlayer distances. The triangle shows a value determined by Lin *et al.* (Ref. 26) for 5.5-ML Fe grown at low temperature on $Cu_3Au(100)$. The small rhombus (Ref. 9) and the small circle (Ref. 8) show experimental data for Fe films on Cu(100).

with increasing film thickness can explain the different step heights determined by STM.[26] Thus our structure determination should be consistent with previously published data and the speculation made by Marcus and Jona.[5]

In conclusion we have shown that the ferromagnetic iron films grow with a strained bcc structure on Cu_3Au. This strain is reduced with increasing film thickness. The magnetic reorientation transition is not related to a structural transformation between fcc and bcc iron but rather occurs in a thickness regime where considerable strain reduction takes place. This structural change is mainly controlled by the elastic properties of the film, the misfit to the substrate, and the interface properties. The transition is observed at slightly larger thicknesses for RT films, which might be attributed to the layer amount of intermixing at the interface, which should increase the overall stress and the onset of dislocation formation. The magnetic reorientation on the contrary has a lower switching thickness for RT films than LT films. The magnetic reorientation is therefore not dominated by the strain reduction. A competition of crystal and shape anisotropy determines the switching thickness. The interface anisotropy can be modified considerably by an intermixing at the interface, which explains the dependence of the magnetic reorientation upon growth temperature.

The prime goal of this study is the characterization of film structure and the correlation of film stress and film structure. Contrary to common expectation and previous studies, no fcc modification was found. This finding, which is at first sight somewhat puzzling can be understood if we consider the different contributions to the total energy mentioned in the Introduction. For the case of pseudomorphic growth, i.e., the film adopts the underlying substrate, the contribution of the film strain can be derived from the elastic constants of the film. If we neglect the interfacial and surface contribution to the total energy, then the condition for the stability of a metastable state on an fcc substrate with lattice constant a is

$$E_{\mathrm{ms}}+\delta E_{\mathrm{ms,\,strain}}\leqslant E_{\mathrm{st}}+\delta E_{\mathrm{st,\,strain}}. \tag{1}$$

This implies that the energy of the metastable state E_{ms}, plus the energy necessary to strain the metastable phase into pseudomorphy on the substrate must be smaller then the sum of the energy of the stable phase E_{st}, plus the energy necessary to strain the metastable phase into pseudomorphy on the substrate. The growth of metastable states is facilitated if the

energy difference between the stable and the metastable phase is small. Furthermore a large misfit between the stable phase and the substrate but a small misfit between the metastable phase and the substrate is requested to stabilize the metastable state. Consider now the different states of iron. From the work of Asada and Terakura[34] we obtain an energy difference of 169 meV between the AFM fcc state and the thermodynamical stable bcc state. For the FM fcc iron the energy difference to bcc iron amounts to 207 meV. To strain FM fcc iron into perfect pseudomorphism on $Cu_3Au(100)$, a strain energy of 15 meV is requested, assuming that the elastic constants of ferromagnetic fcc iron are identical to the constants of AFM fcc iron. While for the bcc phase, a layer strain energy of 89 meV is requested. Nevertheless, the difference in strain energies is smaller than the energy differences of the two states. Hence, bcc iron should be stable on Cu_3Au. Furthermore, the bcc iron films can reduce the strain energy by the formation of misfit dislocations, which explain the observed increase in the in-plane spacing. In conclusion, if we can neglect interfacial and surface contributions to the total energy, then the pseudomorphic bcc iron film should be more favorable than the FM fcc state in agreement with our experimental observation. Our results also indicate that on Rh(100) with a primitive square edge of 2.69 Å the Fe film should be expected to be strained bcc as found by Begley *et al.*[3] On Cu(100) with a lattice spacing of 2.55 Å, on the contrary, the fcc phase is more stable than the bcc phase. The determination of the iron film structure on substrates with lattice constants between 2.55 and 2.65 Å should give an estimate on the role played by the surface and the interfacial contributions to the total energy.

V. SUMMARY

For Fe films with thicknesses up to 53 ML, the structure was determined using measured LEED $I(V)$ data and the comparison with full dynamical calculations. For layer thicknesses of 18 and 53 ML an almost perfect bcc film structure is found, in close agreement with previous studies employing kinematic theory. For small thicknesses of 3.3 and 4.8 ML the iron films also possess a bcc structure but are considerably strained to accommodate the substrate spacing. The conclusion is in line with estimates of the total energy of the iron film. The energy difference between the stable bcc state and the metastable FM fcc state is too large to be compensated by the difference in strain energy for the films. Furthermore our results are in agreement with previous predictions by Marcus and Jona.[5]

ACKNOWLEDGMENTS

This work was supported by the Deutsche Forschungsgemeinschaft (Contract No. Wu 243/2) and the VDI project ''Magnetische Multischichten,'' Grant No. VDI 13 N 6607. We thank W. Moritz for providing the code for the LEED calculations. B.F. gratefully acknowledges the support of the Konrad Adenauer Stiftung.

[1] M. N. Baibich, J. M. Broto, A. Fert, F. Nguyen Van Dau, F. Petroff, P. Eitenne, G. Creuzet, A. Friederich, and J. Chazelas, Phys. Rev. Lett. **61**, 2472 (1988).
[2] G. Binasch, P. Grünberg, F. Saurenbach, and W. Zinn, Phys. Rev. B **39**, 4828 (1989).
[3] F. Jona and P. M. Marcus, Surf. Rev. Lett. **3**, 1285 (1996).
[4] W. D. Nix, Metall. Trans. A **20**, 2217 (1989).
[5] P. M. Marcus and F. Jona, Surf. Rev. Lett. **1**, 15 (1994).
[6] J. Thomassen, F. May, B. Feldmann, M. Wuttig, and H. Ibach, Phys. Rev. Lett. **69**, 3831 (1992).
[7] U. Gradmann, in *Handbook of Magnetic Materials* (Elsevier Science Publishers B.V., Amsterdam, 1993).
[8] S. Müller, P. Bayer, C. Reischl, K. Heinz, B. Feldmann, H. Zillgen, and M. Wuttig, Phys. Rev. Lett. **74**, 765 (1995).
[9] M. Wuttig and J. Thomassen, Surf. Sci. **282**, 237 (1993).
[10] T. Kraft, P. M. Marcus, and M. Scheffler, Phys. Rev. B **49**, 11 511 (1994).
[11] G. L. Krasko and G. B. Olson, Phys. Rev. B **40**, 11 536 (1989).
[12] H. Landskron, G. Schmidt, K. Heinz, K. Müller, C. Stuhlmann, U. Beckers, M. Wuttig, and H. Ibach, Surf. Sci. **256**, 115 (1991).
[13] W. L. O'Brien and B. P. Tonner, Phys. Rev. B **52**, 15 332 (1995).
[14] B. Schirmer and M. Wuttig, Surf. Sci. **399**, 70 (1998).
[15] W. L. O'Brien and B. P. Tonner, Surf. Sci. **334**, 10 (1995).
[16] E. J. Escoria-Aparicio, R. K. Kawakami, and Z. Q. Qiu, J. Appl. Phys. **79**, 4964 (1996).
[17] K. Kalki, D. D. Chambliss, K. E. Johnson, R. J. Wilson, and S. Chiang, Phys. Rev. B **48**, R18 344 (1993).
[18] J. Giergiel, J. Kirschner, J. Landgraf, J. Shen, and J. Woltersdorf, Surf. Sci. **310**, 1 (1994).
[19] M. Stampanoni, A. Vaterlaus, M. Aeschlimann, and F. Meier, Phys. Rev. Lett. **59**, 2483 (1987).
[20] H. Li, Y. S. Li, J. Quinn, D. Tian, J. Sokolov, F. Jona, and P. M. Marcus, Phys. Rev. B **42**, 9195 (1990).
[21] S. D. Bader and E. R. Moog, J. Appl. Phys. **61**, 3729 (1987).
[22] A. M. Begley, S. K. Kim, F. Jona, and P. M. Marcus, Phys. Rev. B **48**, 1786 (1993).
[23] C. Egawa, Y. Tezuka, S. Oki, and Y. Murata, Surf. Sci. **283**, 338 (1993).
[24] U. Gradmann and H. O. Isbert, J. Magn. Magn. Mater. **15-18**, 1109 (1980).
[25] R. Rochow, C. Carbone, Th. Dodt, F. P. Johnen, and E. Kisker, Phys. Rev. B **41**, 3426 (1990).
[26] M.-T. Lin, J. Shen, W. Kuch, H. Jenniches, M. Klaua, C. M. Schneider, and J. Kirschner, Phys. Rev. B **55**, 5886 (1997).
[27] S. H. Lu, J. Quinn, D. Tian, F. Jona, and P. M. Marcus, Surf. Sci. **209**, 364 (1989).
[28] B. Feldmann, B. Schirmer, A. Sokoll, and M. Wuttig, Phys. Rev. B **57**, 1014 (1998).
[29] J. Thomassen, B. Feldmann, and M. Wuttig, Surf. Sci. **264**, 406 (1992).
[30] W. Moritz, J. Phys. C **17**, 353 (1984).
[31] V. L. Moruzzi, J. F. Janak, and A. R. Williams, *Calculated Electronic Properties of Metals* (Plenum, New York, 1978).
[32] J. B. Pendry, J. Phys. C **13**, 937 (1980).
[33] G. Kleinle, W. Moritz, and G. Ertl, Surf. Sci. **238**, 119 (1990).
[34] T. Asada and T. Terakura, Phys. Rev. B **46**, 13 599 (1992); **48**, 17 649 (1993).